Since January 2020 Elsevier has created a COVID-19 resource centre with free information in English and Mandarin on the novel coronavirus COVID-19. The COVID-19 resource centre is hosted on Elsevier Connect, the company's public news and information website.

Computational Biology and Chemistry 88 (2020) 107348

Contents lists available at ScienceDirect

Computational Biology and Chemistry

journal homepage: www.elsevier.com/locate/cbac

Research Article

Design, molecular docking analysis of an anti-inflammatory drug, computational analysis and intermolecular interactions energy studies of 1-benzothiophene-2-carboxylic acid

Abir Sagaama, Noureddine Issaoui*

University of Monastir, Laboratory of Quantum and Statistical Physics LR18ES18, Faculty of Sciences, Monastir 5079, Tunisia

ARTICLE INFO

Keywords:
1-benzothiophene-2-carboxylic acid
anti-inflammatory effect
intermolecular interactions
Rhodanine
molecular docking

ABSTRACT

In this paper, theoretical study on molecular geometry, vibrational, pharmaceutical and electronic properties of the monomeric and dimeric structures of 1-benzothiophene-2-carboxylic acid (2BT) were carried out using B3LYP hybrid functional with 6-311 + + G(d,p) as basis set. The structural study show that the stability of 2BT crystalline structure arising from O-H…O, C-H…O as well as S-H…O hydrogen bonding interactions. Vibrational analysis, for monomer and dimer species, show a good compatibility between experimental and theoretical frequencies. Then, the 1H and 13C NMR chemical shifts were calculated using Gauge Independent Atomic Orbital (GIAO) technical. In addition, the UV-Vis spectrum was simulated in gas phase and in water throughout TD-DFT calculation. The electronic transitions were identified based on HOM-LUMO energies. However, donor-acceptor interactions and charge delocalization has been studied via natural bond orbital (NBO). The nucleophilic and electrophilic site localization is identified by molecular electrostatic potential. Hirshfeld surface analysis has been discussed based on color code demonstrating the various non covalent interactions. Besides, molecular docking analysis was reported to evince the pharmaceutical properties of the studied molecule.

1. Introduction

Heterocyclic compounds which contain nitrogen or/and sulphur atoms considered as flexible scaffolds for experimental drugs design (Patel and Shaikh, 2010). Benzothiophene, takes its origin from the Coffee beans (Spiller, 1998), is one of the aromatic molecules with benzene and five member heterocyclic sulphur-containing rings. Thank to the broad domain of medicinal activities of this family, the benzothiophene derivatives have attracted the attention of many research groups (Ramos et al., 2016; Amr et al., 2010a; El-Miligy et al., 2017). It finds applications in agrochemical and pharmaceutical industries. In this sense, several pharmaceutical drugs are based on benzothiophene compounds have been widely employed in the treatment of diverse diseases. Among these drugs, Raloxifine (Jones et al., 1984) which permit the precaution and therapy of osteoporosis related to woman postmenopausal (Isloor et al., 2010). In addition, the combination between benzothiophene and other ring molecule was heavily used in medicinal application like Ocular hypertensive activities (Graham et al., 1989), analgesic (Wardakhani et al., 2008), anti-inflammatory (Mohamed et al., 2009), antiallergic (Connor et al., 1992), anticancer, antitubercular, antimicrobial and anti-diabetic (Keri et al., 2017). On the other hand, carboxylic group (COOH) of carboxylic acids is responsible for various significant biochemical (Beveridge and Heywood, 1993) and chemical (Pistolis et al., 1995) properties of these molecules, since his ability to train hydrogen bonding interactions. The 1-benzothiophene-2-carboxylic acid possessed antiviral, antifungal and hypotensive activities (Voegtli, 2020) also it treat leukemia.

To the best of our knowledge, no quantum mechanical computations combined with experimental ones for 1-benzothiophene-2-carboxylic acid (2BT) have been published in the literature yet. In this case, the main goal of the present work is the detailed description of 2BT compound via theoretical and experimental study. For calculation, we have employed the DFT theory with B3LYP/6-311 + + G(d,p) basis set. FT-IR, FT-Raman, NMR studies have been carried out and analyzed. The UV-Vis spectroscopic and molecular orbitals analyses have been performed to elucidate electronic charge transfer within studied compound using TD-DFT calculation. Inter and intramolecular interactions in 2BT crystalline structure were investigated by using topological analysis, Hirshfeld surface investigation, molecular electrostatic potential and natural bond orbital. Also the biological activities of the title molecule were performed in order to discover pharmacological properties. For this reason, molecular docking analysis of 2BT were

* Corresponding author.
E-mail address: issaoui_noureddine@yahoo.fr (N. Issaoui).

https://doi.org/10.1016/j.compbiolchem.2020.107348
Received 28 April 2020; Received in revised form 16 July 2020; Accepted 22 July 2020
Available online 27 July 2020

simulated with different proteins, we have used different types (1DLO, 1LCS, 6LU7, 1AOL, 3LN1, 3V92) of enzymes to prove the anti-viral, anti-leukemia as well as anti-inflammatory effect. In addition, to ameliorate to interaction between protein-ligand complexes, we have hybridized our molecule with Rhodanine ring which have good clinical activities. The 2BT-Rhodanine system demonstrates a high inhibitory level compared with 2BT only.

2. Computational details

The molecular structure of 2BT compound has been examined by X-ray diffraction. The crystallographic structure of the molecule mentioned above was obtained from the Cambridge Crystallographic Data Centre (Anon, 2020a). The structural parameters for the most stable conformer of monomeric and dimeric structure of 2BT compound were performed at B3LYP level of theory via 6-311 + + G(d,p) basis set with the help of Gaussian 09 package (Frisch et al., 2009). B3LYP represents the combination between hybrid functional (Becke, 1993a) with Lee-Yang-Parr's correlation functional (LYP) (Lee et al., 1998; Miehlich et al., 1989). Then, vibrational mode assignments were computed on the basis of the potential energy distribution (PED). The 1H and 13C chemical shifts are computed throughout GIAO method (Wolinski et al., 1990) at DFT/B3LYP level of theory with 6-311 + + G(d,p). The atoms in molecule (AIM), reduced density gradient (RDG) for the working compound are plotted by Multiwfn program (Lu and Chen, 2012) with the help of VMD software (Humphrey et al., 1996). The electronic transitions, chemical reactivity descriptors, total density of state (DOS) and UV-Vis theoretical values (in gas and water) of 2BT have been performed by using TD-DFT/6-311 + + G(d,p). The solvent effects were examined via IEF-PCM model. Furthermore, Hirshfeld surface analysis and 2 dimensional fingerprint associated plot were generated through. cif file, which the result of X-ray diffraction, using crystal explorer 3.1 (Wolff et al., 2012). Molecular docking analyses were obtained by using iGEMDOCK (Yang and Chen, 2004), the graphical representations of protein-ligand complex were visualized via Discovery studio (Anon, 2009).

3. Results and discussion

3.1. Molecular geometry

Molecular structural optimization with atomic numbering scheme of monomer and dimer of 2BT carboxylic acid are represented in Fig. 1(1a and 1b). The title compound belongs to C1 point group of symmetry. The geometrical parameters and other properties (energy, dipole moment) are calculated by using DFT (B3LYP) level with 6-311 + + G(d,p) basis set, as shown in Table 1. In the ground state, the minimum energy of our compound is -895.39389 Hartree for the monomer and -1790.53281 Hartree for dimer. The dipole moment values are found to be 2.92 Debye and 0.00 Debye in monomeric and dimeric structure, respectively. The computed and experimental geometrical parameters with Root Mean Square Deviation (RMSD) value are illustrated in Table 1. The RMSD values of bond length (0.0792) and bond angles (2.8355) show a good agreement among calculated and observed data. From this table, we can deduce the presence of strong linear hydrogen bonding; H3…O17 = 177.01° and bond lengths O1-H19 = 1.6696 Å, O17-H3 = 1.6697 Å. Comparing X-ray data values, we can find that almost calculated bond lengths and bond angles are slightly smaller, by the fact that the obtained calculations are carried out in the gas phase while the experimental parameters are reported on the solid phase. As shown on Fig. S1, the crystallographic arrangement of 2BT was ensured by three types of hydrogen bond; O-H…O, C-H…O and S-H…O. The most important bond is O-H…O which responsible to the formation of dimmers, whereas the C-H…O and S-H…O bonds assure the shorter contacts.

3.2. Vibrational analysis

Infrared spectroscopy is a diagnostic tool for determining the nature of the chemical bonds in a molecule (Socrates, 2004). It also makes it possible to obtain important information about inter and intramolecular interactions, on the organization of matter and conformation of the molecule. The experimental infrared and Raman spectrums of 2BT were taken from the literature (Anon, 2020b; Anon, 2020c). The 2BT monomer, fall into C1 point group, possess 18 atoms, consequently it have 48 vibrational normal modes. In order to occur the spectroscopic signature of 2BT carboxylic acid, we carried out a frequency calculation by B3LYP/6-311 + + G(d,p) level. The assignment of the vibration modes is performed using the Veda4 software package building on the Total Energy Distribution (PED). The simulated and observed wavenumbers for the monomer and dimer structures of the title compound combined with infrared intensities, Raman activities and their vibrational assignments (PED) are illustrated in Tables 2 and S1. As clearly shown, in latest tables, the vibrational modes are presented in descending order: from the highest to lowest frequency. Since the experimental spectra are measured in the solid phase whereas the theoretical one are simulated for isolated molecule in the gas phase, therefore there are a difference between these values. For this reason a scaling factor s ($s = \upsilon_{exp}/\upsilon_{calc}$) is introduced to find a good agreement with the experimental frequencies of 2BT. In this work, the harmonic frequencies greater than 1700 cm^{-1} are multiplied by 0.958, while those below 1700 cm^{-1} are multiplied by 0.983 (Sundaraganesan et al., 2005; Karabacak et al., 2008). Furthermore, the duplication of frequencies in dimer spectrum are explained by the presence of symmetric modes since 2BT is considered as centrosymmetric compound. Figs. S2 and S3 illustrate the observed and calculated IR and Raman spectra of 2BT compound. Fig. S4 present, also, the FT-IR spectrum in the range 1775-1550 cm^{-1}. Infrared and Raman spectra are calculated in ground state using B3LYP/6-311 + + G(d,p) level.

3.2.1. COOH modes

The carboxylic acid function is highly polar so it allows the creation of hydrogen bonds with other polar molecules or with polar solvents such as water and alcohols. The O-H group vibrations are the most responsive to the environment; they demonstrate shifts to low frequency regions with an increasing of intensity in hydrogen bonding spectra. This is owing to the formation of H-bond interaction in crystalline structure of the studied compound. The experimental O-H band appear in the range of 3400-3600 cm^{-1}. In the present work, one O-H stretching band was observed at 3590 cm-1 in FT-IR and the calculated value are 3614 for monomer and 3032 cm^{-1} for dimer. From PED, the contribution of this mode is totally stretching (100%). The frequency downshift of νOH vibration in dimer structure is justified by the formation of non covalent interactions, namely O-H…O hydrogen bond. The scaled O-H in-plane bending frequencies occur in the general of 1132-1433 cm^{-1} for monomer and 1352-1663 cm^{-1} for dimer. The experimental bands recorded at 1370, 1300, 1210 and 1140 in FT-IR and at 1280, 1270 and 1253 cm-1 in FT-Raman were assigned to δHOC mode. The increasing of O-H in-plane bending vibration values was explained by the effect of hydrogen bonding interaction resulted by the presence of the carboxylic group. The O-H out of plane bending modes are absent for the title compound. In the other side, the existence of carbonyl group (C = O) is directly related to the highest peak in the infrared spectrum. Generally, the C = O stretching modes occur in the range 1690-1800 cm^{-1} (Issaoui et al., 2017; Issaoui et al., 2015; Issa et al., 2020). It present a strong absorption intensity and very sensitive to any modification in the crystal. The C = O stretching vibration of 2BT molecule is observed at 1750 cm^{-1} in FT-IR spectrum, while the calculated scaled value is found to be 1702 and 1653 cm^{-1} for monomer and dimer structures, respectively. The scaled frequencies 697 and 449 cm^{-1} correspond to the in plan C-O vibration which observed at 705 cm^{-1} in FT-IR spectra. The O-C = O bending vibration is observed

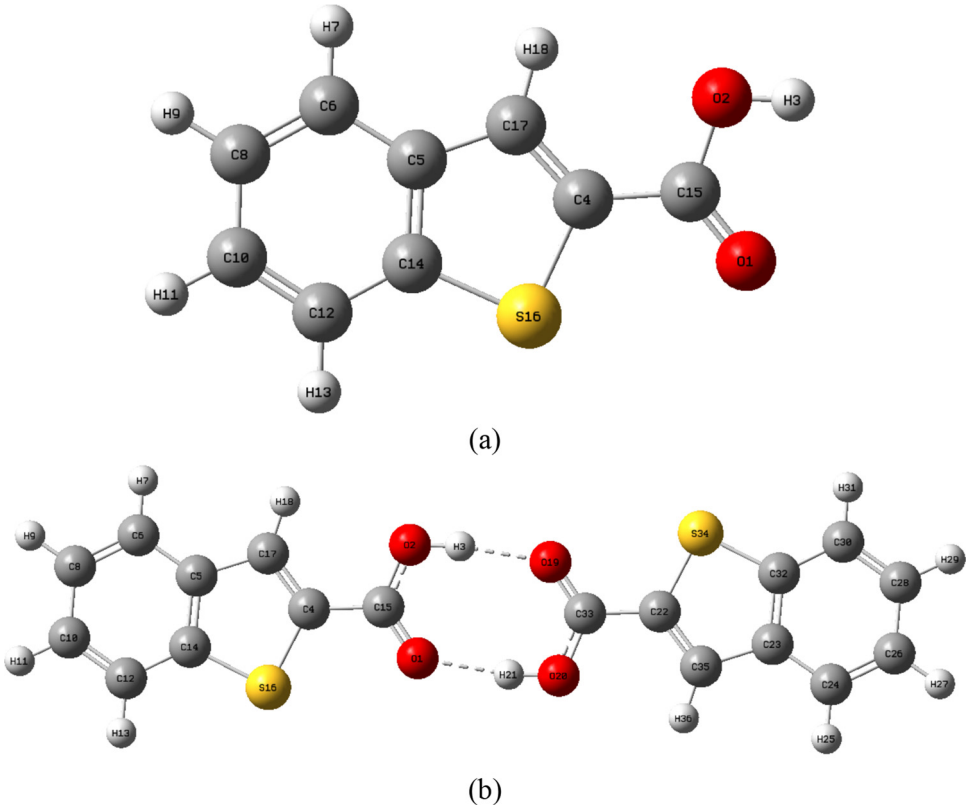

Fig. 1. Molecular structural optimization with atomic numbering scheme of monomer (a) and dimer (b) of 2BT.

at 670 cm^{-1} in FT-IR spectrum and computed at 664 and 579 cm^{-1} with more than 70% PED value, it present deviation about 20 cm^{-1} for dimeric structure. The γOCOC out-of-plane bending vibration was recorded at 770 cm^{-1} and predicted in the range 741-760 cm^{-1} in monomer structure and 747-755 cm^{-1} in dimer one. The νOC and adjacent δHOC vibrations are extremely coupled. These frequencies are generally observed in dimer conformation, it recorded at 1595 cm^{-1} in IR spectrum and computed at 1663 and 1454 cm^{-1}. The hydrogen bond stretching vibration in dimeric specie is calculated at 88 cm^{-1}.

3.2.2. C-C and SC modes

Normally, the C-C stretching vibrations of phenyl group are recorded in the region 1650-1200 cm^{-1} (Muthu and Isac Paulraj, 2012). In our case it is predicted in the 1605-1024 cm^{-1} and 1605-1251 frequency

Table 1
Theoretical and experimental parameters of 2BT compound.

Structural parameters	Monomer	Exp	Dimer	Structural parameters	Monomer	Exp	Dimer
Bond Length(Å)							
O1-C15	1.209	1.229(2)	1.226	C6-C8	1.383	1.372(2)	1.394
O2-H3	0.968	0.86(2)	0.999	C8-H9	1.083	0.950	1.082
O2-C15	1.358	1.316(2)	1.316	C8-C10	1.407	1.405(2)	1.395
C4-C15	1.467	1.466(2)	1.474	C10-H11	1.084	0.950	1.083
C4-S16	1.757	1.740(2)	1.735	C10-C12	1.386	1.375(2)	1.403
C4-O17	1.364	1.405(4)	1.378	C12-H13	1.083	0.950	1.083
C5-C6	1.408	1.404(2)	1.408	C12-C14	1.398	1.400(2)	1.391
C5-O14	1.418	1.412(2)	1.416	C14-S16	1.750	1.732(1)	1.753
C5-O17	1.430	1.548(4)	1.424	C17-H18	1.081	0.950	1.081
C6-H7	1.084	0.950	1.083	**RMSD**	**0.0792**	-	**0.0811**
Bond Angles(°)							
H3-O2-C15	106.678	111(1)	110.397	H11-C10-C12	119.396	119.4	119.089
C15-C4-S16	118.623	117.8(1)	119.194	C10-C12-H13	120.711	120.9	120.141
C15-C4-C17	128.288	123.2(2)	127.622	C10-C12-C14	118.353	118.3(1)	118.146
S16-C4-C17	113.087	119.1(2)	113.182	H13-C12-C14	120.934	120.8	121.439
C6 -C5-C14	119.101	119.1(1)	119.086	C5-C14-C12	121.298	121.2(1)	121.636
C6-C5-C17	129.125	127.1(2)	129.069	C5-C14-S16	111.748	112.8(1)	111.479
C14C5-C17	111.773	113.8(2)	111.844	C12-C14-S16	126.953	126.0(1)	126.884
C5-C6-H7	119.842	120.3	120.063	O1-C15-O2	122.660	124.0(1)	125.215
C5-C6-C8	119.469	119.5(1)	119.400	O1-C15-C4	124.979	121.5(1)	121.362
H7-C6-C8	120.688	120.3	120.536	O2-C15-C4	112.360	114.6(1)	113.422
C6-C8-H9	119.897	119.5	119.706	C4-S16-C14)	90.428	90.25(7)	90.761
C6-C8-C10	120.666	120.9(1)	120.598	C4-C17-C5	112.962	104.0(2)	112.732
H9-C8-C10	119.436	119.6	119.695	C4-C17-H18	122.671	128.0	122.384
C8-C10-H11	119.493	119.5	119.778	C5-C17-H18	124.366	128.0	124.883
C8-C10-C12	121.110	121.1(1)	121.131	**RMSD**	**2.8355**	-	**2.5555**

Table 2
Experimental and theoretical vibrational wavenumbers of 2BT.

Mode	Experimental frequency (cm-1)		Theoretical frequencies (cm-1)		IR intensity	Raman activity	Assignments with PED (%)
	FT-IR	FT-Raman	Unscaled	Scaled			
1	3590	-	3772	3614	126.88	172.9	νOH (100)
2	3500	-	3217	3082	0.19	88.16	νCH (99)
3	3090	-	3194	3060	14.25	321.67	νCH (95)
4			3186	3052	14.17	73.07	νCH (96)
5			3176	3043	3.12	121.7	νCH (96)
6			3168	3035	0.16	33.34	νCH (95)
7	1750	-	1777	1702	538.32	286.92	νOC (82)
8	1595	-	1633	1605	9.35	130.15	νCC (63), δHOC (13)
9	1570	1337	1599	1572	14.26	30.23	νCC (63)
10	1510	1320	1557	1531	87.17	384.99	νCC (65)
11	1410	1305	1489	1464	5.77	25.6	νCC (28), δHCC (47)
12			1458	1433	27.56	64.47	δHOC (10), δHCC (45)
13	1370	1280	1375	1352	65.32	7.99	νCC (39), δHOC (17)
14	1300	1270	1347	1324	81.07	12.9	νCC (48), δHOC (26)
15			1338	1315	0.58	133.47	νCC (38), δHCC (17), δCCC (12)
16	1210	1253	1273	1251	8.85	25.04	νCC (18), δHOC (13), δHCC (19)
17	-	1240	1230	1209	50.92	3.79	δHOC (18), νCH (23)
18			1187	1167	17.29	11.03	δHCC (65)
19	1140	-	1166	1146	351.17	52.74	νCC (21), δHOC (20), νCH (38)
20			1152	1132	3.51	38.13	νCC (24), δHOC (51)
21			1081	1063	26.21	36.76	νSC (49), δCCC (15)
22			1042	1024	29.41	45.13	νCC (67), δHCC (11)
23	1005	-	1024	1007	70.77	5.72	νSC (70)
24			996	979	0	0.06	τHCCH (91)
25			960	944	2.15	0.13	τHCCH (89)
26	880	-	889	874	12.09	1.9	τHCCC (87)
27			873	858	0.17	5.19	νSC (12), νSC (10), δCCC (47)
28			859	844	0.76	0.3	τHCCS (91)
29	770	-	773	760	80.66	0.25	τHCCC (24), γOCOC (61)
30			754	741	7.71	0.17	τHCCC (64), γOCOC (26)
31			732	720	9.5	22.68	δCCC (16), νSC (51)
32	720	-	725	713	25.08	0.08	τCCCC (80)
33	705	-	709	697	9	1.85	νSC (54), δCCO (14)
34	670	-	675	664	33.61	7.08	δOCO (74)
35			589	579	26.08	3.79	δOCO (78)
36	610	-	574	564	12.27	1.69	τHOCC (92)
37	560	-	545	536	66.08	1.41	τHOCC (88)
38			497	489	0.85	11.53	δCSC (66)
39			467	459	31.82	0.12	γSCCC (87)
40			457	449	4.95	5.24	νSC (19), δCCO (59)
31			426	419	0.02	0.32	τCCCC (80)
42			340	334	0.55	0.58	δCCC (70)
43			327	321	2.92	4.91	νCC (13), δCCC (32), νSC (17)
44			252	248	0.16	0.27	γCCSC (94)
45			197	194	0.05	0.15	τCCCS (88)
46			138	136	2.47	0.31	δCCC (85)
47			87	86	0.47	1.74	τCCCC (92)
48			69	68	0.54	0.07	τCCCO (93)

(ν- stretching; δ- in plane bending; γ- out of plane bending; τ- torsion).

ranges respectively for the monomer and dimer structure. In the phenyl ring, these bands are expected at 1595, 1570, 1510, 1410, 1370, 1300, 1210, 1140 cm^{-1} in IR spectra and 1337, 1320, 1305, 1280, 1270, 1253 cm^{-1} in Raman spectrum. The six δCCC in plan vibration of 2BT, calculated at B3LYP/6-311 + + G(d,p) level, are in the 321-1315 cm^{-1} frequency range. The peak occur at 720 cm^{-1} in infrared spectra is assigned to CCCC torsion mode; the computed values of τCCCC band are 419 and 86 cm^{-1}.

In thiophene ring, the band observed at 1005 cm^{-1} in infrared is related to νSC stretching mode, the scaled values are equal 1007, 858, 697, 449 cm^{-1}. While, the calculated value of δCSC in plan bending is 488.80 cm^{-1}. The vibrations for the out of plane bending deformations of the studied molecule are found at 248 and 459 cm^{-1}.

3.2.3. C-H modes

The aromatic structures prove the presence of C-H stretching wavenumbers ranging from 3000-3100 cm^{-1} (Sagaama et al., 2020). Habitually, the C-H stretching vibrations are expected along with strong Raman intensity. In our case, four hydrogen atoms left around the phenyl ring give rise to four νCH modes, are predicted in the frequency range of 3060-3035 cm^{-1} with contribution more than 95%. One of these pure vibrations is obtained at 3090 cm^{-1} in infrared spectrum with high PED contribution (95%). The carbon-hydrogen stretching mode of the thiophene ring was observed in the experimental IR spectrum at 3500 cm^{-1} and computed for monomer and dimer, indicating slight difference about 5 cm^{-1}. Besides, the in plan C-H bending modes generally observed in the region 1000-1300 cm^{-1} in substituted benzene vibrations occur in the area 750-1000 cm^{-1} (Becke, 1993b; Muthu and Uma Maheswari, 2012). In addition, the in plan bending vibrations are found to be 1410, 1210, in infrared spectra and 1305, 1253 cm^{-1} in FT-Raman. Whereas, the calculated values are predicted in the range 1024-1433 cm^{-1} and 1573-1035 cm^{-1} for monomer and dimer, respectively.

3.3. NMR study

Thank to his large sensibility to the conformational changement, the

Table 3
Theoretical chemical shifts δ of ^{13}C and ^{1}H for monomer structure obtained in DMSO solvent.

Atoms	δ theoretical (ppm)			
	Monomer		Dimer	
	Gas phase	DMSO	Gas phase	DMSO
	TMS B3LYP/6-311 + G (2d,p) GIAO	TMS B3LYP/6-311 + G (2d,p) GIAO	TMS B3LYP/6-311 + G (2d,p) GIAO	TMS B3LYP/6-311 + G (2d,p) GIAO
C15	184.91	187.75	171.74	173.39
C4	165.74	165.11	161.53	155.53
C5	164.60	164.59	148.08	159.36
C14	152.12	151.62	158.72	148.94
C10	151.48	152.70	145.28	121.24
C17	149.96	152.33	150.51	150.32
C8	148.24	149.36	139.33	138.99
C6	139.93	140.78	142.57	124.54
C12	133.88	134.85	139.40	148.94
H3	9.72	10.76	13.41	6.98
H18	8.95	9.21	7.89	7.42
H11	8.22	8.46	7.34	6.70
H9	8.10	8.31	7.19	6.05
H13	8.06	8.31	7.40	6.70
H7	7.91	8.14	7.55	6.05

NMR spectroscopy is a useful tool for the structural analysis of the organic molecules. It furnishes information about the various atomic types existing in the crystal. In the present work, the ^{1}H and ^{13}C NMR theoretical spectra of monomer and dimer were carried out in gas phase and DMSO solvent throughout the B3LYP/6-311 + + G(d,p) method. Then, the ^{1}H and ^{13}C NMR isotropic shielding were computed via "Gauge-Independent Atomic Orbital (GIAO) (Ditchfield, 1972; Barfield and Fagerness, 1977) method and TMS B3LYP/6-311 + G (2d,p) and TMS HF/6-31 G(d) as references. The corresponding theoretical results of ^{1}H and ^{13}C NMR for monomer and dimer in gas phase and DMSO are collected in Table 3.

Generally, the ^{13}C isotropic shifts of organic compounds are ranging from 10 to 200 ppm (Kalinowski et al., 1988). For aromatic ring, the carbon NMR chemical shifts are lying in the region 115-150 ppm (Noureddine et al., 2020). Then,^{13}C NMR spectrum of compounds based on benzothiophene revealed signals corresponded to carbon atoms of thiophene ring at 127.34, 129.05, 136.85 and 143.40 ppm (Amr et al., 2010b). The studied compound has nine carbon atoms; C15, C4, C5, C14, C10, C17, C8, C6 and C12, their shift values in DMSO solvent are 187.75, 165.11, 164.59, 151.62, 152.70, 152.33, 149.36, 140.78, 134.85 ppm, respectively. The theoretical ^{13}C NMR spectrum makes out that the highest deshielded signal is found to be 184.91 (gas)/187.75 (DMSO) ppm, because this carbon (C15) is attached to the carboxylic acid group (COOH) which responsible to the establishment of hydrogen bonding interactions. Besides, the C6 carbon atom has the second greatest chemical shift since is related to the oxygen atom of phenyl ring with chemical shift value 139.39 in gas and 140.78 in DMSO. In the organic molecule, the aromatic proton shifts are recorded in the range of 7.00-8.00 ppm (John Xavier and Dinesh, 2014). The ^{1}H chemical shifts of benzothiophene derivatives are observed in the range 6.95-7.99 ppm (Isloor et al., 2010). Mainly, the hydrogen atoms are concentrated on the outskirt of the molecule, thus their isotropic shifts are heavily sensitive to intermolecular interactions. In the monomeric structure of 2BT, there are four hydrogen atoms linked to phenyl ring, one hydrogen attached to thiophene ring and one linked to the hydroxyl group. Passing from monomer to dimer conformation, clear differences have been shown in chemical shift values especially in C5, C8, C15 and H3, owing to the existence of H-bond interactions. The weaker chemical shift value of H3 witch attached to the carboxylic functional group (COOH) demonstrate the formation of hydrogen bond; O2-H3…O17 previously seen.

3.4. Topological studies

Atoms in molecule approach analysis is carried out to discover intermolecular interaction among neighboring atoms. To examine the topological characteristics at BCP point, we computed the electron density (ρ), Laplacien (Δρ), and electronic energy density (H), which correspond to the sum of kinetic energy (G) and the electronic potential energy V as well as interaction energy $E_{int} = V/2$ (Gatfaoui et al., 2020). Generally, the electronic density values of H-bond ranging from 0.0070 to 0.0302 a.u and it matching Laplacien values are vary between 0.024 and 0.139 a.u. As it is shown in Fig. 2, molecular schematic visualization of monomeric and dimeric structure demonstrates the existence of a bond critical points (BCP) among hydrogen donor (O2-H3 and O18-H19) and hydrogen acceptor (O1 and O17) groups. However, in 2BT monomer there are two ring critical points (RCP) due to the presence of phenyl and thiophene rings. After dimerisation, we observe another type of critical points, new critical point (NRCP) owing to the formation of H-bond interactions. All topological parameters at critical point are collected in Table 4. This latter show a high interaction energy value of hydrogen bonds at BCP point witch found to be -417.79 KJ/mol, demonstrating the strong H-bonds. Then, the sign of electronic energy density (H) at BCP is an indicator of non-covalent interaction category; electrostatic dominant if $H < 0$ or covalent dominant if $H > 0$ (Tahenti et al., 2020). We can note from Table 7 that only at the level of hydrogen critical points the interaction is electrostatic dominant.

On the other hand, the reduced density gradient is a useful technical to identify the type of interaction; H-bond, Van der Waals or steric interaction throughout a color code. The blue color associate to stabilize the hydrogen bond, the green and red ones are employed, respectively, to depict destabilize VDW and repulsion steric interactions. The Fig. 3 shows the different intermolecular interactions present in crystal structure of our molecule. The variation of RDG vs. sign (λ2) ρ is represented in Fig. S5. The spike with negative value (-0.047 a.u), indicating strong hydrogen bonding interactions which mostly owing to O-H…O bonds. The reduced gradient spikes ranging from 0.01 to 0.04 a.u, representing strong repulsion steric effect, while the spikes near zero denotes the Van der Waals interactions. These results are in good agreement with those previously seen in the structural study.

3.5. UV-Vis and frontier molecular orbitals analysis

In quantum chemistry, a TD-DFT calculation is considered as a standing theoretical technical. It is a reasonable approach compared to semi-empirical and ab-initio calculation methods (Guillauumont and Nakamura, 2000). The absorption wavelength for UV is ranging from 190 to 400 nm, whereas for the visible it is found in the region 400-800 nm. In this work, the UV-Vis spectrum of our compound has been conducted by Time-Dependent Density Functional Theory (TD-DFT) in

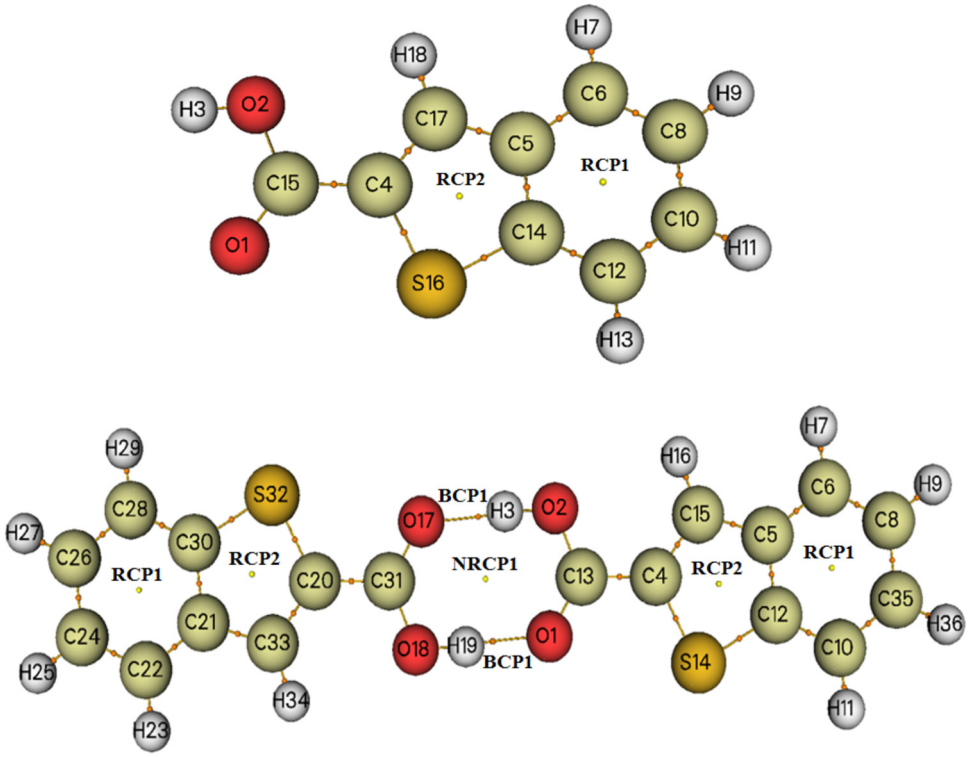

Fig. 2. AIM schematic visualization of monomeric and dimeric structures.

gas phase and water. The graphical representation UV-Vis spectra of 2BT carboxylic acid were shown in Fig. S6. The excitation energy (E), the absorption wavelength (λ), the oscillator force (f) and the contribution of the different electronic transitions are collected in Table 5. Besides, UV-Vis spectra predict maximum absorption peaks at 280 nm (f = 0.2919 a.u) in gas phase and 287 nm (f = 0.3979 a.u) in water. It can be assigned to the H-1→ L (81%) and H-1→L (87%) electronic transitions. While, the second calculated band is found to be 317 and 327 nm in phase gas and water, respectively. The great intensity of peaks in water solvent demonstrates the high solubility of the studied compound in water, which considered as an advantage in drug industries. These peaks correspond to the electronic transition between the ground state (HOMO) and the first excited state (LUMO). In this context, The HOMO and LUMO frontier orbitals constitute a convenient tool for defining the chemical, molecular as well as electrical activities. The HOMO orbital is deemed as a nucleophile while the LUMO orbital is considered as an electrophile (Zhuo et al., 2012; Prashanth et al., 2016). The delocalized π orbital (HOMO) as an electron donor represents the ability to donate an electron, while the localized π orbital (HOMO) depicts the ability to accept an electron. Then, the HOMO-LUMO energy calculations of 2BT molecule were performed using DFT theory level via B3LYP/6-311 + +G(d,p). As shown in Table 6, the calculated energy values of the title compound are found to be E_{HOMO} = -6.54 eV, E_{LUMO} = -2.19 eV and gap energy $E_{HOMO\text{-}LUMO}$ = -4.35 eV. The value of the gap energy is an important parameter, since this value related deeply to the reactivity of the compound, it vary inversely proportional to the chemical reactivity. Based on HOMO and LUMO energies, the ionization potential (I) and electronic affinity (A) are computed using the following equations; I = $-E_{HOMO}$ and A = $-E_{LUMO}$. Then, the electronegativity (χ) and chemical hardness are given by; χ = (I + A)/2 and η = (I + A)/2. Whereas, the chemical potential and global softness are defined as the negative of electronegativity (μ = - χ) and the inverse of hardness (S = 1/η), respectively. The electrophilicity index Ψ is calculated by the following relation; $\Psi = \mu^2/2\eta$. The ionization potential (I), electronic affinity (A), electronegativity (χ), chemical hardness (η), global softness (S), chemical potential (μ) and electrophilicity (Ψ) of 2BT have been collected in Table 9. The hardness and softness parameters are useful to determine the stability and the reactivity of molecule. The high ionization energy value designates high stability and weak ionization energy point to molecular reactivity of the studied compound. In our case, the monomeric structure considered as hard compared with the dimmeric structure. This property is proved by the large gap energy (-4.35 eV) and the small value of softness (0.23 eV^{-1}). In addition, the dimer structure is treated as a strong electrophile since it characterized by a high value of electrophilicity (13.35 eV), while the monomer form is considered as nucleophile. The 3D representation of HOMO and LUMO frontier molecular orbitals are plotted via GausView program, as illustrated in Fig. 4. In this 3D plot, the red color describe the positive phase and the green one corresponds to the negative region. In the other hand, the neighboring orbitals can

Table 4
Topological parameters of the title compound at critical point.

	Critical points	ρ (u.a)	Δρ (u.a)	H(r) (u.a)	G(r) (u.a)	V(r) (u.a)	E_{int} (kJ mol^{-1})
Monomer	RCP1	0.0213	0.1554	0.0074	0.0314	−0.0239	-
	RCP2	0.0376	0.2290	0.0055	0.0517	−0.0462	-
Dimer	BCP1	0.2819	−0.9714	−0.2806	0.0378	−0.3185	−417.9796
	RCP2	0.0212	0.1547	0.0074	0.0312	−0.0238	-
	RCP2	0.0379	0.2312	0.0054	0.0523	−0.0468	-
	NRCP1	0.0079	0.0310	0.0068	0.0068	−0.0059	-

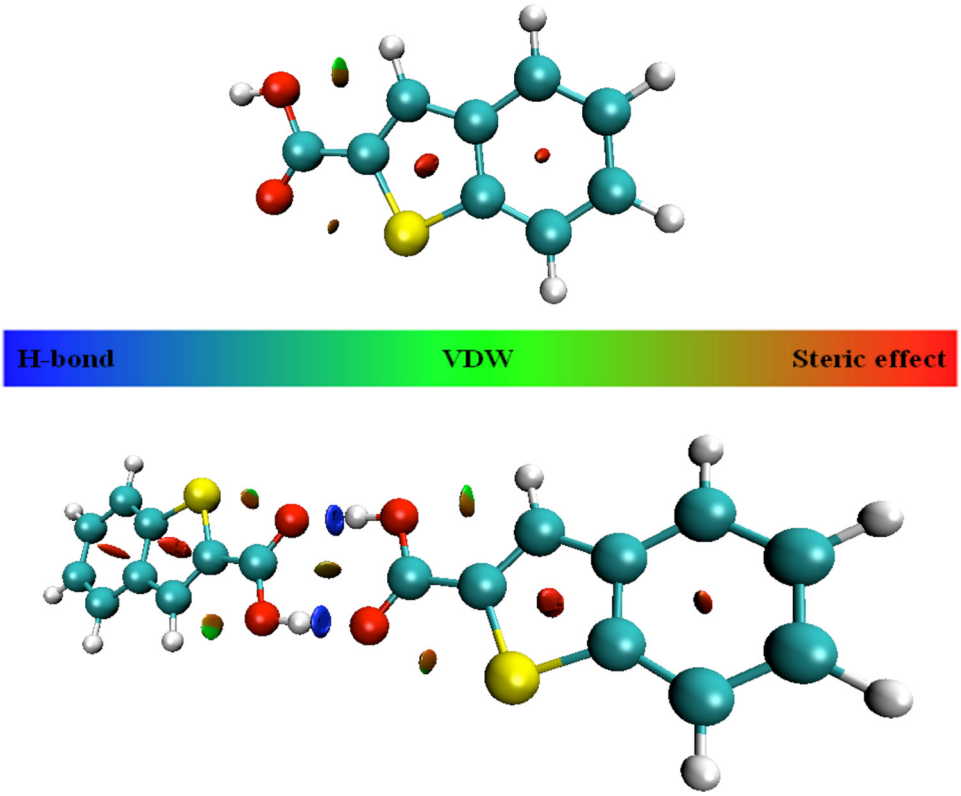

Fig. 3. RDG isosurface with intermolecular interaction-coding for crystalline structure of 2BT.

Table 5
The excitation energy (E), the absorption wavelength (λ) and the oscillator force (f) of 2BT compound.

Gas phase				Water			
E (eV)	λ (nm)	f (a.u)	Major contribution	E (eV)	λ (nm)	f (a.u)	Major contribution (%)
3.90	318	0.0694	H→L (88%)	3.81	325	0.1039	H→L (91%)
4.41	281	0.2919	H-1→L (81%)	4.31	287	0.3979	H-1→L (87%)
4.72	262	0.0000	H-2→L (96%)	4.88	254	0.0000	H-3→L (96%)

H = HOMO; L = LUMO; L + 1 = LUMO + 1; etc.

Table 6
Monomeric and dimeric chemical parameters of 2BT carboxylic acid.

Energy (eV)	Monomer	Dimer
HOMO	−6.54	−9.30
LUMO	−2.19	−5.33
HOMO-LUMO	−4.35	−3.97
Chemical parameters		
Ionization potential (I)	6.54	9.30
Electronic affinity (A)	2.19	5.33
Electronegativity (χ)	−4.36	−7.31
Chemical hardness(η)	2.17	1.98
Global softness (S)	0.23	0.25
Chemical potentiel (μ)	4.36	7.31
Electrophilicity (ψ)	4.37	13.35

present degeneration of energy levels; consequently the consideration of HOMO and LUMO orbitals is insufficient to get a real description of frontier molecular orbitals (FMOs). Wherefore, the density of state (DOS) depending in Mulliken charge population analysis is computed and generated via GaussSum. 3 software (O'Boyle et al., 2008). The DOS diagram reveals the composition as well as the chemical contribution of molecular orbitals, as clearly seen in Fig. S7. This latter demonstrate the occupied and virtual orbitals and the gap energy.

3.6. Molecular electronic potential (MEP) and natural bond analysis (NBO)

The molecular electronic potential map give a visual representation of charge distribution and offer information related to nucleophilic and electrophilic sites localization. In this work, the molecular electronic potential surfaces were plotted at the B3LYP/6-311 + + G(d,p) level of theory. The molecular electrostatic potential representations of monomeric and dimeric forms are illustrated in Fig. 5. The MEP surfaces of monomer and dimer conformer are plotted using a color code ranging from -5.749 $.10^{-2}$ to 5.749 $.10^{-2}$ and -3.134 $.10^{-2}$ to 3.134 $.10^{-2}$, respectively. The electrophilic sites are characterized by positive potential and mapped with blue color. Conversely, the nucleophlic sites possess a negative potential value, are represented with red color. While, the green color is employed to determine neutral regions. As clearly seen, from Fig. 5, the highest negative potential values are recorded on oxygen atoms of the carbonyl group (C = O) whereas the stronger positive potential value are localized on the hydrogen atoms especially that belong to the hydroxyl group (O-H). The findings results are in a good agreement with our previous analysis and confirm the formation of hydrogen bonded interaction among monomer units.

In the other side, the Fig. S8 illustrates the atomic charge distribution. The Mulliken charges of each atom were computed at B3LYP/6-311 + + G(d,p) basis set. O1 and O2 oxygen atoms of carboxylic group

Table 7
Stabilization energy E(2) of inter and intramolecular interactions of 2BT monomer and dimer in term natural bond orbitals.

		Monomer			Dimer		
Donneur(i)	Accepteur(j)	E(2)	E(j)-E(i)	F (i,j)	E(2)	E(j)-E(i)	F (i,j)
π (C4 - C17)	π * (O1- C15)	22.11	0.28	0.072	23.02	0.27	0.073
π (C5 - C14)	π *(C6 - C8)	16.51	0.30	0.064	14.81	0.31	0.062
π (C6 -C8)	π *(C5 - C14)	19.40	0.27	0.068	20.06	0.27	0.069
LP (1) O1	σ (C4 - C15)	2.30	1.14	0.046	1.75	1.15	0.038
LP (2) O2	π *(O1- C15)	48.48	0.35	0.120	9.50	1.13	0.093
LP (2) O1	σ (O 2 - C15)	29.88	0.65	0.126	26.17	0.67	0.120
LP (2) S16	π * (C4 - C17)	25.01	0.24	0.071	24.86	0.24	0.071
LP (2) S16	π *(C5 - C14	22.32	0.26	0.070	22.00	0.26	0.070
LP (1) O1	σ*(O18 - H19)	-	-	-	6.04	1.42	0.083
LP (2) O1	σ*(O18 - H19)	-	-	-	5.94	0.98	0.070
LP (1) O17	σ*(O2 – H3)	-	-	-	6.68	1.42	0.087
LP (2) O17	σ*(O2– H3)	-	-	-	6.58	9.98	0.074

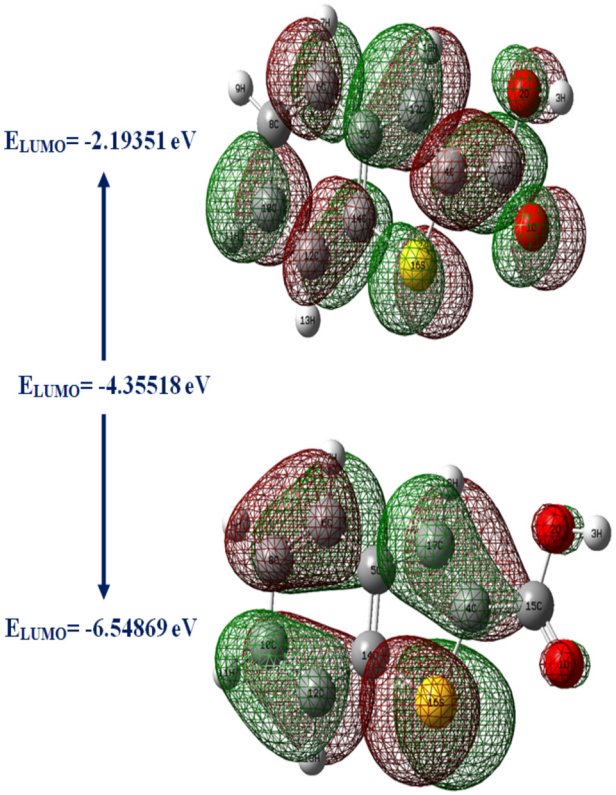

Fig. 4. HOMO and LUMO frontier orbitals of 2BT molecule (monomer).

and S16 sulfur atom of thiophene ring possess the highest Mulliken charge, while the hydrogen atom H3 has the largest positive charge. It can be noted that all hydrogen atoms in 2BT compound present positive Mulliken charge.

In the aim of investigating intra and intermolecular interactions in molecules, the natural bond orbital (NBO) was used. It reveals a practical basis studying electronic charge transfer and possible donor-acceptor interaction within molecular systems. Also, it demonstrates delocalization of electronic density from occupied donor orbital to vacant acceptor orbital. In the current study, the NBO analysis was carried out via Gaussian 09 program to study 2BT stability (monomer and dimer). The stabilization energy $E^{(2)}$, the donor (i) and acceptor (j) associated to the delocalization terms (i and j) by the following equation: $E^{(2)} = \Delta E_{ij} = q_i F(i,j)/(E_i\text{-}E_j)$, where E_i and E_j are the diagonal elements, q_i is donor orbital occupancy and $F_{i,j}$ is off diagonal NBO Fock matrix element. In addition, the second-order perturbation theory computed for monomer and dimer of 2BT compound are collected in Table 7. The NBO calculation show a clear differences among monomer and dimer forms, this difference are explained by the training of hydrogen bonding interactions in dimeric form among oxygen lone pairs (LP) and σ*(O-H) antibonding orbitals. The $E^{(2)}$ values of LP(1)O1→σ*(O18-H19), LP(2)O1→σ*(O18-H19), LP(1)O17→σ*(O2-H3) and LP(2)O17→σ*(O2-H3) are obtained as 6.04, 5.94, 6.68 and 6.58 kcal/mol, respectively.

3.7. Hirshfeld surfaces investigation

In order to discover interactions between atoms and their function in building up crystal structure of molecule, Hirshfeld surface (HS) analysis was conducted by using crystal explorer program. 3D Hirshfeld surface along with 2D fingerprint were used to think about intermolecular contacts, introducing hydrogen bonding as well as π- π interactions. The 3 dimensional surfaces of the studied compound are plotted over d_{norm}, d_i, d_e, shape index, curvedness and fragment patch, as it is shown in Fig. S9. The properties of d_{norm} (-0.7491-1.0895 Å), d_i (0.6425-2.6088 Å), d_e (0.6426-2.5769 Å), shape index (-1-1 Å), curvedness (-4 - 4 Å) and fragment patch (0-13 Å). The d_{norm} map was plotted by using red-white-blue code where the red contours represent shorter contact with distance less than the sum of VDW radii ($d_i + d_e$), the blue regions correspond to longer contacts, including that the closest external atom has a distance value bigger than $d_i + d_e$ Van der Waals radii. While, contacts with a distance equal to $d_i + d_e$ radii are represented by white color. As it is shown in Fig. 6, the bright red areas on the d_{norm} plots mark the presence of strong O-H…O hydrogen bond, whereas the weaker H-bond interactions (C-H…O) are represented as minor visible light red region and the S-H…O are very weak since it plotted with white spots. In this context, the H3, H21, O1, O2, O19, O20 atoms of carboxylic group make out their participation in H-bond of O-H…O type. In the other hand, the d_e plot represents the nearest distance from the nucleus external to the surface and d_i plot denotes the nearest distance from the nucleus inter to the surface of the compound (Spackman and McKinnon, 2002). Depending in d_e and d_i, the fingerprint plots give a schematic representation of intermolecular interaction among atoms pair. The red spots wrapped with yellow crowns in d_e and d_i surfaces demonstrate the formation of H-bond interactions (O-H…O), and the H…H interactions are visualized as yellow regions. This yellow color show that the hydrogen atoms of H…H interactions are inside Hirshfeld surface. The longer contacts in d_e and d_i plots are represented with blue color. However, in shape index plot, the π-π stacking interactions are mapped through red triangles indicating concave areas outside HS. Whereas, the convex regions in ring carbon atoms which localized inside the surface are represented by blue triangles (Feng et al., 2016). In curvedness surface, the green planar surface surrounded with blue outline proves the presence of π…π stacking interactions in crystal lattice (Muthuraja et al., 2016).

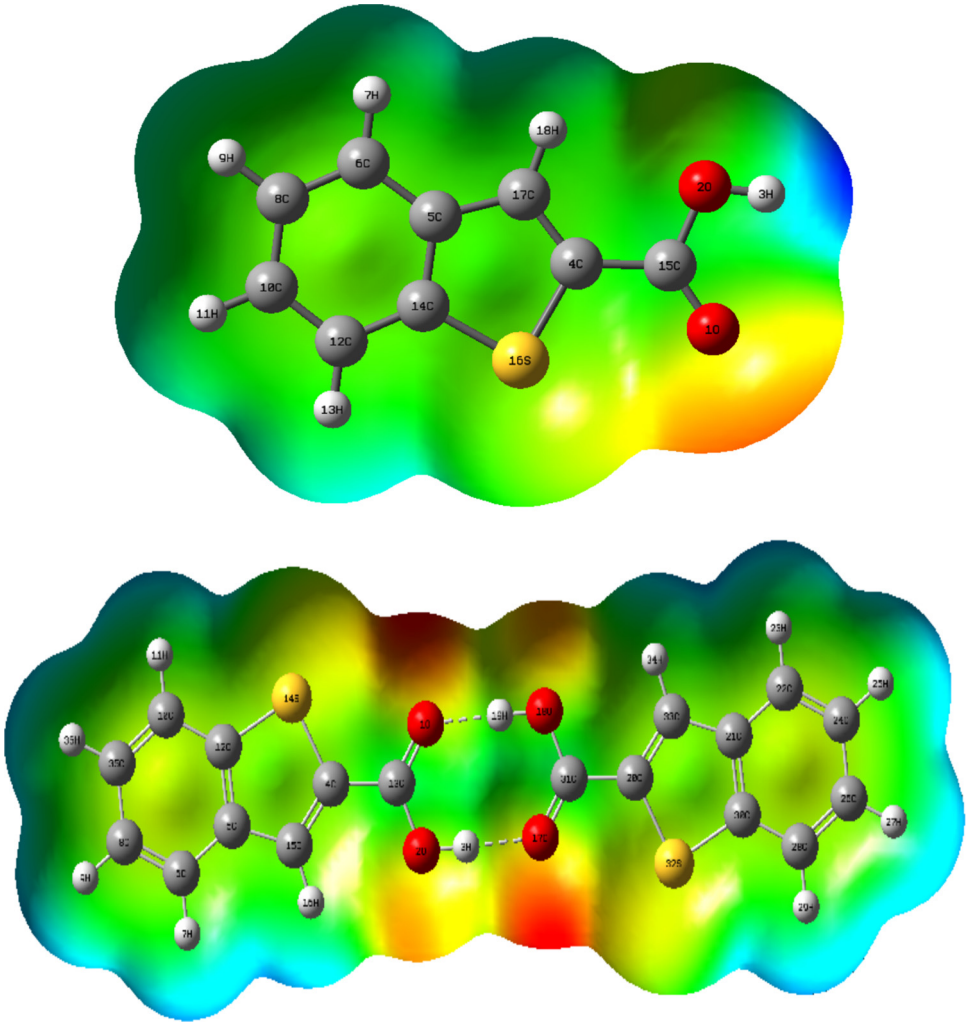

Fig. 5. MEP surfaces for monomeric and dimeric structure of 2BT compound.

As clearly seen from Fig. S10, the largest contribution is due to the H…H interactions amounting to 41.8% which is because the existence of abundance hydrogen atoms in 2BT crystal. Besides, the O…H/H…O contacts are shown as spikes with 23.2% of the total Hirshfeld surface. The H…C/C…H interactions holds 13.4% of the totality of the Hirshfeld surface at $d_i + d_e = 3$ Å bigger than the sum of VDW radii of carbon (1.70 Å) and hydrogen (1.09 Å) atoms. Further, the contribution percentage of C…C is found to be 11.2% owing to the existence of thiophene and phenyl rings. S…H/H…S contacts with $d_i + d_e = 2.98$ Å contribute by 3.9% to the total surface, responsible for the formation of S-H…O weak hydrogen bonding interaction.

3.8. Molecular docking analysis

Molecular docking is an excellent tool to analyze the protein-ligand interactions, which considered as a crucial area in structure drug designing. To discover the biological activities of 2BT carboxylic acid, molecular docking computation has been carried out using iGEMDOCK program (Yang and Chen, 2004) and Discovery studio (Anon, 2009) software as interface visualization. Here, we employed the accuracy setting; population size (800), generations (80) and number of solutions (10). In this part, we serve to discover three biological properties, antiviral and leukemia treatment as well as anti-inflammatory effect of the title compound by using two proteins for each property. Human immunodeficiency virus type 1 (1DLO) (Hsiou et al., 1996), Bat SARS-like coronavirus (6LU7) (Barnett et al., 2003), Feline leukemia virus (1LCS) (Jin et al., 2020), Friend murine leukemia virus (1AOL) (Fass et al., 1997), COX-2 (3LN1) (Wang et al., 2010) and 5-LOX (3V92) (Gilbert et al., 2012) are the enzymes used to investigate antiviral, anti-leukemia as well as anti-inflammatory activities, respectively. In this sense, Human immunodeficiency virus type 1 (HIV-1) is responsible to largest acquired immunodeficiency syndrome. However, Bat SARS-like coronavirus is a novel beta coronavirus which cause respiratory illness. Feline leukemia virus and Friend murine leukemia virus are viruses generate one of the most dangerous cancers for human, namely leukemia. Whereas, COX-2 and 5-LOX inflammatory proteins generate disorders of the gastric mucosa and undesirable physiological effects, respectively.

The energetic calculations of the molecular docking simulation are tabulated in Table 8 and the matching docking positions are visualized from Fig. 7. The binding energy of 3NL1, 1DLO, 3V92, 1LCS, 6LU7 and 1AOL are equal to -81.44, -79.33, -72.48, 71.84, -68.37 and -67.84 kcal/mol. From Table 4, it can be observed that the totality of interaction energy is H-bond and VDW type. The binding score of 2BT in COX-2 protein considered the highest total energy presenting great hydrogen bond (-66.34 kcal/mol) and the biggest electrostatic bond (-5.12 kcal/mol). In Human immunodeficiency virus type 1, the 2BT ligand possess large binding energy -79.33 kcal/mol with the stronger H-bond (-69.65 kcal/mol) and the weaker VDW interaction (-7.75 kcal/mol). Whereas, 1AOL have the lowest binding ligand with -67.84 kcal/mol value. In addition, the Feline leukemia virus corresponds to the stronger VDW and electrostatic interactions with values found to be

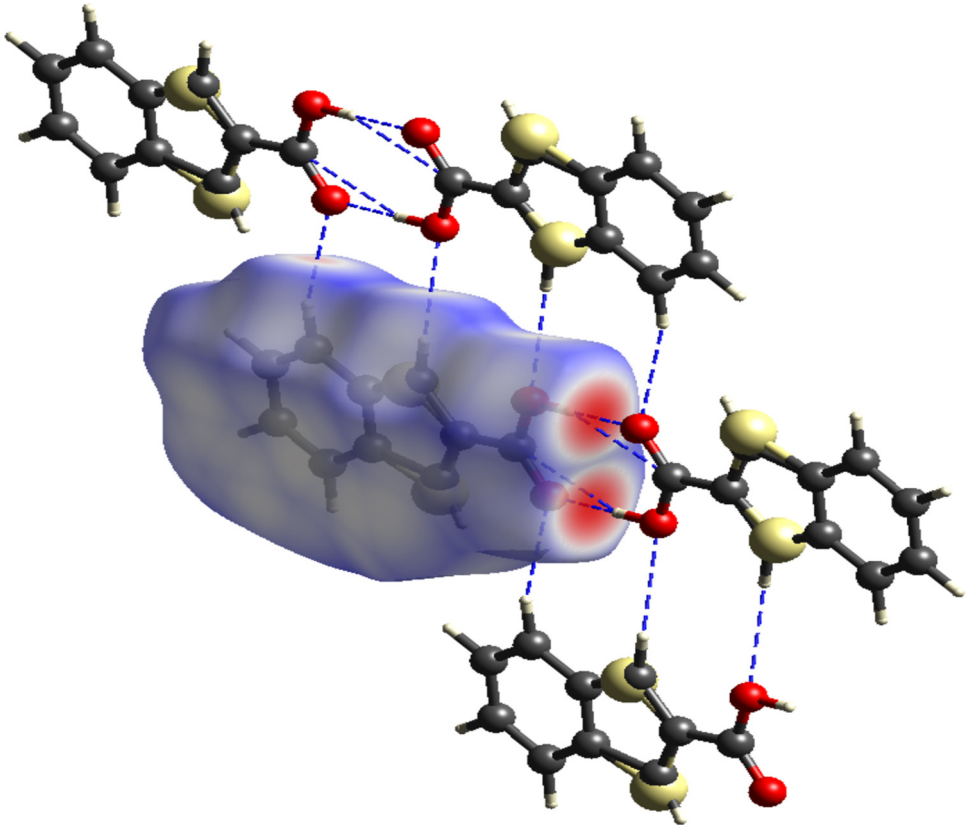

Fig. 6. d_{norm} schematic representation of various hydrogen bonding interactions in 2BT crystal structure.

Table 8
Molecular docking calculation of the title compounds with various proteins.

Protein Name	Code	Interaction energy E_{tot}(kcal/mol)	$E_{H\text{-}bond}$	E_{VDW}	E_{Elect}	Residues	Bond length	Interaction category
COX-2	3LN1	−81.44	−66.34	−9.98	−5.12	C:HIS:374	3.68	H-bond
						C:TRP:373	4.07	H-bond
						C:HIS:193	3.61	Hydrophobic
						C:HIS:372	5.31	Hydrophobic
							2.95	Other
						C:ALA:188	4.78	Hydrophobic
Human immunodeficiency virus type 1	1DLO	−79.33	−69.65	−7.75	−1.93	A-LYS-223	2.87	H-bond
						A-TYR-318	3.97	H-bond
							3.87	
						A-TYR-118	3.55	H-bond
						A-HIS-235	4.46	Hydrophobic
						A-VAL-106	3.68	Hydrophobic
						A-PRO-225	3.44	H-Bond
5-LOX	3V92	−72.48	−61.86	−10.62	0	A:ALA:404	3.00	H-bond
						A:ALA:405	2.86	H-bond
						A:PHE:402	3.03	H-bond
						A:ARG:401	3.93	Hydrophobic
							4.59	Hydrophobic
						A:ILE:167	5.23	Hydrophobic
Feline leukemia virus	1LCS	−71.84	−53.46	−15.58	−2.8	A-ARG-87	2.93	H-Bond
							2.61	
							3.52	
						A-CYS-90	5.76	Other
						A-GLY-91	3.08	Other
						A-ALA-85	5.43	Hydrophobic
Bat SARS-like coronavirus	6UL7	−68.37	−53.31	−15.06	0	A-THR-111	2.60	H-bond
							3.09	
						A-THR-111	3.10	H-bond
Friend murine leukemia virus	1AOL	−67.84	−56.61	−13	−1.78	A-ASP-21	3.09	H-Bond
						A-LEU-48	2.02	H-Bond
						A-GLY-20	3.70	H-Bond
						A-THR-221	3.81	Hydrophobic
							3.77	H-Bond
						A-PRO-53	4.23	Hydrophobic
							4.37	Hydrophobic

Table 9
Molecular docking calculation of 2BT-Rhodanine system with various proteins.

Protein Name	Code	Interaction energy E_{tot} (kcal/mol)	$E_{H\text{-}bond}$	E_{VDW}	E_{Elect}
COX-2	3LN1	−98.37	−91.06	−7.30	0
5-LOX	3V92	−91.07	−72.01	−15.10	−3.95
Human immunodeficiency virus type 1	1DLO	−86.23	−74.29	−11.29	0
Bat SARS-like coronavirus	6UL7	−85.09	−74.51	−8.71	−1.86
Feline leukemia virus	1LCS	−82.22	−70.03	−10.65	−1.53
Friend murine leukemia virus	1AOL	−76.90	−63.29	−10.07	−3.52

-15.58 and -2.8 kcal/mol, respectively. As it is shown on Figs. 8 and S11, the intermolecular interactions were represented by scattered lines and coded by a color code. The degradation of green color represent the most important bonds (H-bond and VDW interaction), the yellow one characterize the π-sulfur or sulfur-X bond. While, the purple and pink colors correspond to the transitions among orbitals (π-σ, π-Alkyl). 2D interaction representations of 2BT in 3NL1, DLO, 3V92, 1LCS, 6LU7 and 1LAO proteins are generated in Fig. 8. As can be seen from 2D map, there are three types of hydrogen bond; conventional hydrogen bond, carbon hydrogen bond and π-donor hydrogen bond. The C-HIS-374 and C-TRP-373 amino acids of 3NL1-2BT complex enter in hydrogen bonding interactions, demonstrating bond lengths 3.68 and 4.07 Å, respectively. Then, the other residues enter into hydrophobic bonds with distance lay between 3.61-5.31 Å. Subsequently, in 2BT compound A-LYS-223, A-TYR-318 and A-PRO-225 amino acid residues of 1DLO enzyme that are implicated in hydrogen bonding, having bond lengths range in 2.87- 4.46 Å. Whereas, the A-HIS-235 (4.46 Å) and A-VAL-106 (3.68 Å) participated with 2BT ligand in hydrophobic bonds. For 3V92-2BT, the A-ALA-404, A-ALA-405, and A-PHE-402 form H-bond interactions with carbonyl group and thiophene ring. The bond lengths of these residues range from 3-3.03 Å. The other residues are implicated in

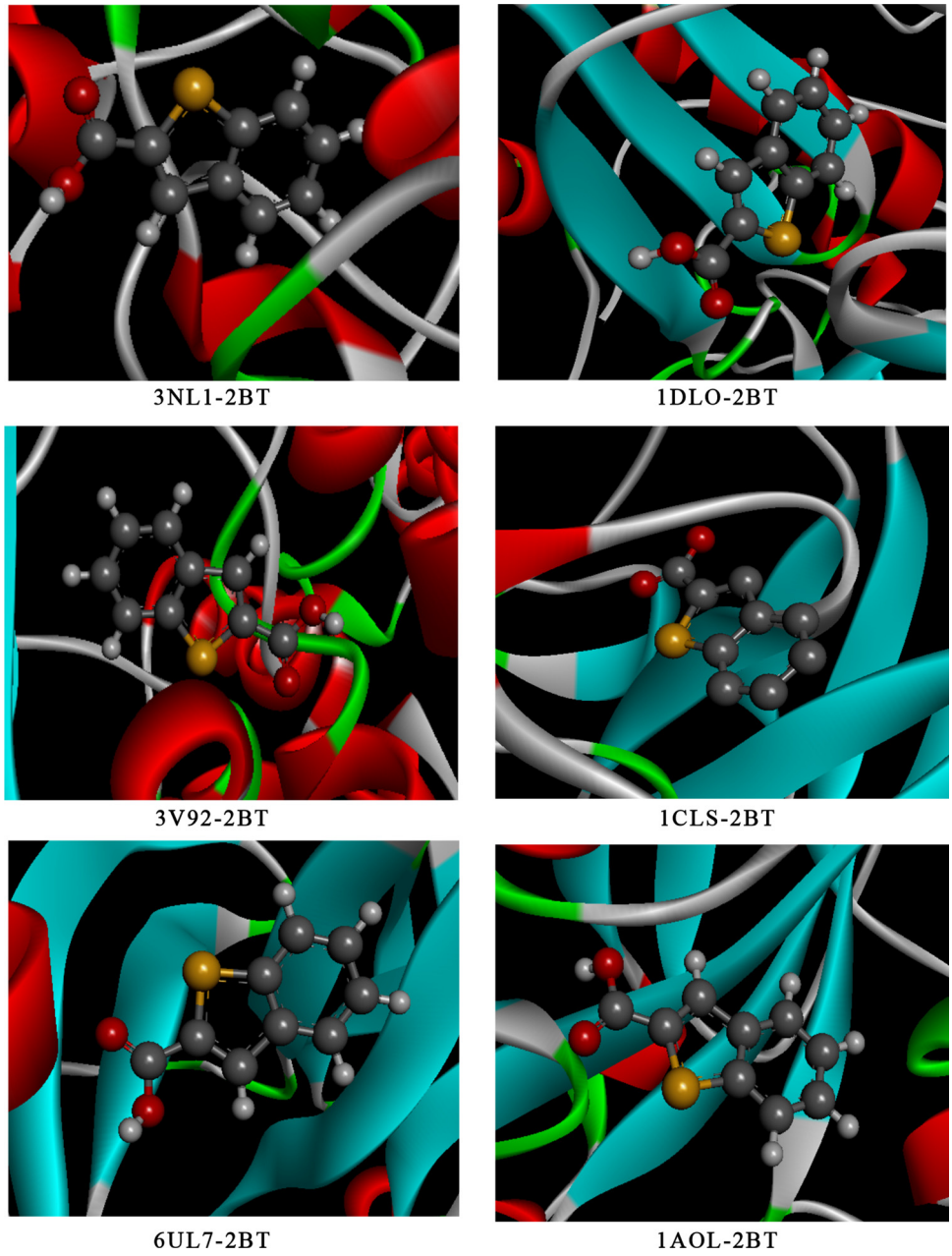

Fig. 7. The best poses of 2BT in 3NL1, 1DLO, 3B92, 1LCS, 6LU7 and 1LAO proteins.

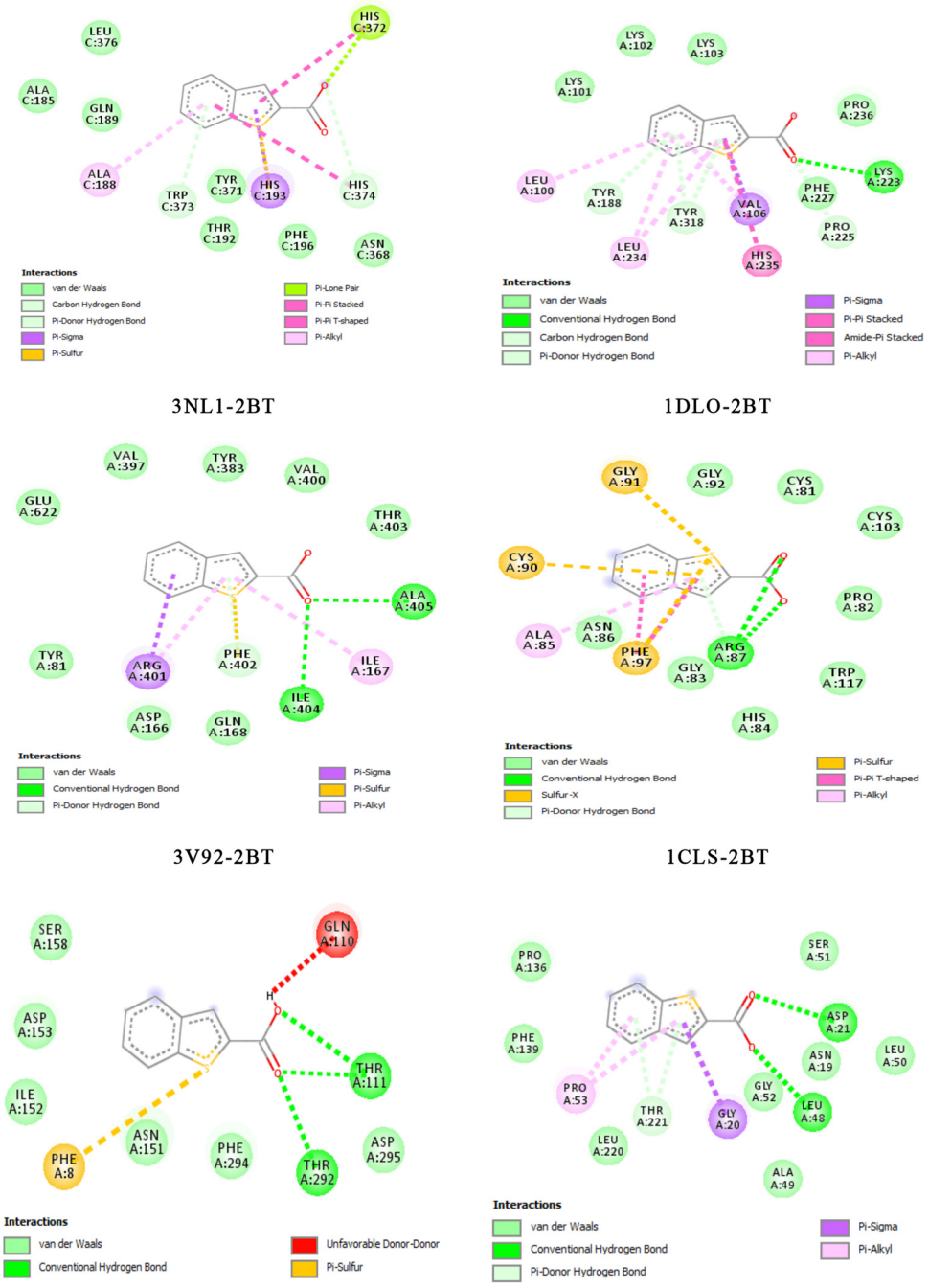

Fig. 8. 2D interaction representation of 2BT with the six proteins.

hydrophobic interactions. Concerning 1LCS-2BT complex, A-ARG-87 form three hydrogen bonds, two with carboxylic group and one with the thiophene ring, marking distance values 2.93, 2.61 and 3.52 Å. Also, our ligand interacts with ACY-90 and A-GLY-91 in sulfur bond and with A-ALA-85 in hydrophobic interaction. The following amino coronavirus residues; A-THR-111 as well as A-THR-292 formed three hydrogen bonding interactions with the studied compound. A-THR interact with carbonyl group, including bond lengths 2.60 and 3.10 Å. Whereas, only A-THR-111 interact with hydroxyl group of carboxylic acid. For 1AOL-2BT system, A-ASP-21, A-LEU-48, A-GLY-20 and A-THR-221 interact with 2BT ligand forming hydrogen bonding interaction with bond lengths 3.09, 2.02, 3.70 and 3.77 Å. While the other residues are involved in hydrophobic interaction; A-THR-221 (3.81 Å), A-PRO-53 (4.23 and 4.37 Å). However, the hydrogen bonding surfaces for the various proteins are represented in Fig. S12. For 1DLO-2BT and 6LU7-2BT interactions, the carbonyl group of carboxylic acid participates as an electron acceptor and the hydroxyl group plays the role of an electron donor, conversely in 3NL1, 3V92, 1LCS- 2BT and 1-AOL complexes. While, the benzothiophene group involve like donor-acceptor electron simultaneously in the six systems. These acceptor-donor contacts were accountable in hydrogen bond training. According to these results, the interaction between 3NL1 and 2BT is deeply stronger than the other ones.

In the other hand, Rhodanine have several biological activities like antimycobacterial, antibacterial, antidiabetic, antifungal, antineoplastic, pesticidal, anti-infective (Inamori et al., 1992; Taniyama

Table 10
Comparative study between COX-2, 5-LOX proteins and different ligands.

		E_{tot} (kcal/mol)	$E_{H\text{-}bond}$	E_{VDW}	E_{Elect}
COX-2	2BT	−81.4	−66.34	−9.98	−5.12
	2BT-Rhodanine	−98.37	−91.06	−7.30	0
	Celecoxib	−116.76	−102.88	−13.88	0
5-LOX	2BT	−72.48	−61.86	−10.62	0
	2BT-Rhodanine	−91.07	−72.07	−15.10	−3.95
	Meclofenamic	−89.62	−80.87	−8.75	0

et al., 1959; Singh et al., 2004; Frankov et al., 1985). It also shows anti–human immunodeficiency virus (HIV), antimalarial activities and antitubercular. Consequently, we desire to evaluate the biological activities of 2BT-Rhodanine in front of various proteins. The Fig. S13 presents the optimized structure of 2BT-Rhodanine. In the case of inflammatory COX-2 and 5-LOX proteins we compare the result of our complex (2BT-Rhodanine) with commercial drugs celecoxib and meclofenamic acid, respectively (Fig. S14). The comparison between Tables 8 and 9 demonstrate that passing from 2BT to 2BT-Rhodanine, the interaction energy of the six proteins were increased especially for 5-LOX enzyme which amplified with more than -18 kcal/mol. The docking calculation revealed that 2BT-Rhodanine complex has good binding score especially in the case of COX-2 and 5-LOX. As can be easily seen in Table 10, the binding energy to COX-2 demonstrate score = -98, 37 kcal/mol which was weaker compared to celecoxib (-116.77 kcal/mol). While, the total energy of 5-LOX enzyme is found to be -91.68 kcal/mol which slightly higher than meclofenamic acid (-89.26 kcal/mol).

The molecular docking findings demonstrate the biological properties of the title compound against COX-2, HIV-1, 5-LOX, coronavirus and leukemia diseases, indicating the promoter inhibition capacity of 2BT ligand especially for COX-2 and Human immunodeficiency virus type 1 (HIV-1). In addition, molecular hybridation combining benzothiophene and Rhodanine show that this system considered as a potential inhibitor against COX-2 and 5-LOX.

4. Conclusion

In this paper, molecular structure of 2BT compound has been optimized via quantum chemical calculation using B3LYP/6-311 + + G(d,p) level of theory. Molecular optimization results and experimental data show good correlation. The experimental vibrational spectra were analyzed, indicating a good correlation with calculated ones. The different techniques have been used to prove the existence of intermolecular interactions; hydrogen bonds (O-H…O, C-H…O and S-H…O), Van der Waals interactions as well as steric effect. However, the molecular frontier orbital approach permits us to estimate chemical reactivity based on gap energy value. Then the UV-Vis spectrum analysis proves that the title compound is soluble in water which considered as beneficial in drug industry designing. Besides, from docking results we can conclude that our molecule can be a competitive dual COX-2/5-LOX as well as HIV-1 virus inhibitors. In addition the hybridization of our compound with Rhodanine raises the inhibitory properties of 2BT.

Declaration of Competing Interest

The authors declare that they have no known competing financial interests or personal relationships that could have appeared to influence the work reported in this paper.

CRediT authorship contribution statement

Abir Sagaama: Conceptualization, Data curation, Writing - original draft, Visualization, Investigation. **Noureddine Issaoui:** Supervision, Software, Validation, Methodology, Writing - review & editing.

Acknowledgement

This work was supported by the Ministry of Higher Education and Scientific Research of Tunisia.

Appendix A. Supplementary data

Supplementary material related to this article can be found, in the online version, at doi:https://doi.org/10.1016/j.compbiolchem.2020.107348.

References

Amr, A.E.G.E., Sherif, M.H., Assy, M.G., Al-Omar, M.A., Ragab, I., 2010a. Antiarrhythmic, serotonin antagonist and antianxiety activities of novel substituted thiophene derivatives synthesized from 2-amino-4, 5, 6, 7-tetrahydro-N-phenylbenzo [b] thiophene-3-carboxamide. European journal of medicinal chemistry 45, 5935–5942.
Amr, A.E.G.E., Sherif, M.H., Assy, M.G., Al-Omar, M.A., Ragab, I., 2010b. Antiarrhythmic, serotonin antagonist and antianxiety activities of novel substituted thiophene derivatives synthesized from 2-amino-4, 5, 6, 7-tetrahydro-N-phenylbenzo [b] thiophene-3-carboxamide. European journal of medicinal chemistry 45 (12), 5935–5942.
Discovery Studio 4.5 Guide. Accelrys Inc., San Diego. http://www.accelrys.com.
https://www.ccdc.cam.ac.uk/(CCDC-N° 950133).
https://webbook.nist.gov.
https://pubchem.ncbi.nlm.nih.gov.
Barfield, M., Fagerness, P., 1977. J. AM. Chem. Soc. 119, 8699–8711.
Barnett, A.L., Wensel, D.L., Li, W., Fass, D., Cunningham, J.M., 2003. Structure and mechanism of a coreceptor for infection by a pathogenic feline retrovirus. Journal of virology 77, 2717–2729.
Becke, A.D., 1993a. J. chem. Phys. 98, 5648–5652.
Becke, D., 1993b. J. Chem. Phys. 98, 5648.
Beveridge, A.J., Heywood, G.C., 1993. Biochemistry 32, 3325–3333.
Connor, D.T., Cetenko, W.A., Mullican, M.D., Sorenson, R.J., Unangst, P.C., Weikert, R.J., Adolphson, R.L., Kennedy, J.A., Thueson, D.O., Wright, C.D., Conroy, M.C., 1992. J. Med. Chem. 35, 958.
Ditchfield, R., 1972. J. Chem. Phys. 56, 5688–5691.
El-Miligy, M.M., Hazzaa, A.A., El-Messmary, H., Nassra, R.A., El-Hawash, S.A., 2017. New hybrid molecules combining benzothiophene or benzofuran with rhodanine as dual COX-1/2 and 5-LOX inhibitors: synthesis, biological evaluation and docking study. Bioorganic chemistry 72, 102–115.
Fass, D., A.Davey, R., Hamson, C.A., Kim, P.S., Cunningham, J.M., Berger, J.M., 1997. Structure of a murine leukemia virus receptor-binding glycoprotein at 2.0 angstrom resolution. Science 277, 1662–1666.
Feng, C., Zhang, D., Chu, Z.J., Zhao, H., 2016. Dimeric complexes of transition metal based on azole nucleating ligands involving hydrogen bonding interactions. Polyhedron. 115, 288–296.
Frankov, A., Kirillov, M.V., Sokolova, T.N., Skupskaya, R., Kharitonovich, A.N., 1985. Chizhev- skaya II, Synthesis and pharmacological properties of alkyl derivatives of 3-carbox- yalkylrhodanine. Khim. Farm. Zh. 19, 943–946.
Frisch, M.J., Trucks, G.W., Schlegel, H.B., Scuseria, G.E., Robb, M.A., Cheeseman, J.R., Scalmani, G., Barone, V., Mennucci, B., Petersson, G.A., Nakatsuji, H., Caricato, M., Li, X., Hratchian, H.P., Izmaylov, A.F., Bloino, J., Zheng, G., Sonnenberg, J.L., Hada, M., Ehara, M., Toyota, K., Fukuda, R., Hasegawa, J., Ishida, M., Nakajima, T., Honda, Y., Kitao, O., Nakai, H., Vreven, T., Montgomery Jr., J.A., Peralta, J.E., Ogliaro, F., Bearpark, M., Heyd, J.J., Brothers, E., Kudin, K.N., Staroverov, V.N., Kobayashi, R., Normand, J., Raghavachari, K., Rendell, A., Burant, J.C., Iyengar, S.S., Tomasi, J., Cossi, M., Rega, N., Millam, N.J., Klene, M., Knox, J.E., Cross, J.B., Bakken, V., Adamo, C., Jaramillo, J., Gomperts, R., Stratmann, R.E., Yazyev, O., Austin, A.J., Cammi, R., Pomelli, C., Ochterski, J.W., Martin, R.L., Morokuma, K., Zakrzewski, V.G., Voth, G.A., Salvador, P., Dannenberg, J.J., Dapprich, S., Daniels, A.D., Farkas, Ö., Foresman, J.B., Ortiz, J.V., Cioslowski, J., Fox, D.J., 2009. Gaussian 09, Revision C.01. Gaussian, Inc., Wallingford C.T.
Gatfaoui, S., Sagaama, A., Issaoui, N., Roisnel, T., Marouani, H., 2020. Synthesis, experimental, theoretical study and molecular docking of 1-ethylpiperazine-1, 4-diium bis (nitrate). Solid State Sci., 106326.
Gilbert, N.C., Rui, Z., Neau, D.B., Waight, M.T., Bartlett, S.G., Boeglin, W.E., et al., 2012. Conversion of human 5-lipoxygenase to a 15-lipoxygenase by a point mutation to mimic phosphorylation at Serine-663. The FASEB Journal 26, 3222–3229.
Graham, S.L., Shepard, K.L., Anderson, P.S., Baldwin, J.J., Best, D.B., Christy, M.E., Freedman, M.B., Gautheron, P., Habecker, C.N., 1989. J. Med. Chem. 32, 2548–2554.
Guillauumont, D., Nakamura, S., 2000. Calculation of the absorption wavelength of dyes using timedependent density-functional theory (TD-DFT). Dyes Pigm. 46, 85–92.
Hsiou, Y., Ding, J., Das, K., Clark Jr, A.D., Hughes, S.H., Arnold, E., 1996. Structure of unliganded HIV-1 reverse transcriptase at 2.7 Å resolution: implications of conformational changes for polymerization and inhibition mechanisms. Structure 4, 853–860.
Humphrey, W., Dalke, A., Schulten, K., 1996. VMD - Visual Molecular Dynamics. J. Molec. Graphics 14 (1), 33–38.
Inamori, Y., Muro, C., Tanaka, R., Adachi, A., Miyamotoand, K., Tsujibo, H., 1992.

Phytogrowthinhibitory activity of sulfur-containing compounds. I. Inhibitory activities of thiazoli- dine derivatives on plant growth. Chem. Pharm. Bull. 40, 2854–2856.
Isloor, A.M., Kalluraya, B., Pai, K.S., 2010. Synthesis, characterization and biological activities of some new benzo [b] thiophene derivatives. European journal of medicinal chemistry 45, 825–830.
Issa, T.B., Sagaama, A., Noureddine, I., 2020. Computational study of 3-thiophene acetic acid: Molecular docking, electronic and intermolecular interactions investigations. Computational Biology and Chemistry, 107268.
Issaoui, N., Ghalla, H., Brandán, S.A., Bardak, F., Flakus, H.T., Atac, A., Oujia, B., 2017. Experimental FTIR and FT-Raman and theoretical studies on the molecular structures of monomer and dimer of 3-thiopheneacrylic acid. J. Mol. Struct. 1135, 209–221.
Issaoui, N., Ghalla, H., Muthu, S., Flakus, H.T., Oujia, B., 2015. Molecular structure, vibrational spectra, AIM, HOMO–LUMO, NBO, UV, first order hyperpolarizability, analysis of 3-thiophenecarboxylic acid monomer and dimer by Hartree–Fock and density functional theory. Spectrochimica Acta Part A: Molecular and Biomolecular Spectroscopy 136, 1227–1242.
Jin, Z., Du, X., Xu, Y., Deng, Y., Liu, M., Zhao, Y., et al., 2020. Structure of Mpro from COVID-19 virus and discovery of its inhibitors. bioRxiv. .
John Xavier, R., Dinesh, P., 2014. Vibrational spectra, monomer, dimer, NBO, HOMO, LUMO and NMR analyses of trans-4-hydroxy-L-proline. Spectrochimica Acta Part A: Molecular and Biomolecular Spectroscopy 128, 54–68.
(a) C.D. Jones, M.G. Jevnikar, A.J. Pike, M.K. Peters, L.J. Black, A.R. Thompson, J.F. Falcone, J.A. Clements, J. Med. Chem. 27 (1984) 1057–1066; (b) V.C. Jordan, J. Med. Chem. 46 (2003) 883–908; (c) V.C. Jordan, J. Med. Chem. 46 (2003) 1081–1111.
Kalinowski, H.O., Berger, S., Brawn, S., 1988. Carbon-13 NMR spectroscopy. John Wiley and Sons, Chichester.
Karabacak, M., Coruh, A., Kurt, M., 2008. FT-IR, FT-Raman, NMR spectra, and molecular structure investigation of 2,3-dibromo-N-methylmaleimide: a combined experimental and theoretical study. J. Mol. Struct. 892, 125e131.
Keri, R.S., Chand, K., Budagumpi, S., Somappa, S.B., Patil, S.A., Nagaraja, B.M., 2017. An overview of benzo [b] thiophene-based medicinal chemistry. European journal of medicinal chemistry 138, 1002–1033.
Lee, C., Yang, W., Parr, G.R., 1998. Phys. Rev. B 37, 785–1489.
Lu, T., Chen, F., 2012. Multiwfn: A multifunctional wavefunction analyzer. J. Comput. Chem. 33, 580–592.
Miehlich, B., Savin, A., Stoll, H., Preuss, H., 1989. Chem. Phys. Lett. 157, 200–406.
Mohamed, A.A.R., Shehab, M.A., El-Shenawy, S.M., 2009. Monatsh. Chem. 140, 445–450.
Muthu, S., Isac Paulraj, E., 2012. Solide state Sci. 14, 476.
Muthu, S., Uma Maheswari, J., 2012. Spectrochim. Acta, Part A: Mol. Biomol. Spectrosc. 92, 154.
Muthuraja, P., Sethuram, M., Shanmugavadivu, T., Dhandapani, M., 2016. Single crystal Xray diffraction and Hirshfeld surface analyses of supramolecular assemblies in certain hydrogen bonded heterocyclic organic crystals. J. Mol. Struct. 1122, 146–156.
Noureddine, O., Gatfaoui, S., Brandan, S.A., Sagaama, A., Marouani, H., Issaoui, N., 2020. Experimental and DFT studies on the molecular structure, spectroscopic properties, and molecular docking of 4-phenylpiperazine-1-ium dihydrogen phosphate. Journal of Molecular Structure 1207, 127762.
O'Boyle, N.M., Tenderholt, A.L., Langner, K.M., 2008. Cclib: a library for package independent computational chemistry algorithms. J. Comp. Chem. 29, 839–845.
Patel, N.B., Shaikh, F.M., 2010. Sci. Pharm. 78, 753–765.
Pistolis, G., Paleos, C.M., Malliaris, A., 1995. J. Phys. Chem. 99, 8896–8902.
Prashanth, J., Ramesh, G., Laxman Naik, J., Ojha, Jai Kishan, Venkatram Reddy, B., 2016. Molecular geometry, NBO analysis, Hyperpolarizability and HOMO-LUMO energies of 2-azido-1-phenylethanone using Quantum chemical calculations. Materials Today: Proceedings 3, 3761–3769.
Ramos, F., Flores, H., Rojas, A., Hernández-Pérez, J.M., Camarillo, E.A., Amador, M.P., 2016. Experimental and computational thermochemical study of benzofuran, benzothiophene and indole derivatives. the Journal of Chemical Thermodynamics 97, 297–306.
Sagaama, A., Noureddine, O., Brandán, S.A., Jarczyk-Jędryka, A., Flakus, H.T., Ghalla, H., Issaoui, N., 2020. Molecular docking studies, structural and spectroscopic properties of monomeric and dimeric species of benzofuran-carboxylic acids derivatives: DFT calculations and biological activities. Com. Biol. Chem. 87, 107311.
R. Singh, U.V. Ramesh, D. Goff, G. Laidig, S.D. Issakani, J. Huang, D.G. Payan. WO Pat 2004043955, 2004.
Socrates, G., 2004. Infrared and Raman characteristic group frequencies: tables and charts. John Wiley & Sons.
Spackman, M.A., McKinnon, J.J., 2002. Fingerprinting intermolecular interactions in molecular crystals. CrystEngComm 4, 378–392.
Spiller, M.A., 1998. In: Spiller, G.A. (Ed.), Caffeine. CRC Press, Boca Raton.
Sundaraganesan, N., Illakiamani, S., Saleem, H., Wojciechowski, P.M., Michalska, D., 2005. FT-Raman and FT-IR spectra, vibrational assignments and density functional studies of 5-bromo-2-nitropyridine. Spectrochim. Acta A Mol. Biomol. Spectrosc. 61, 2995e3001.
Tahenti, M., Gatfaoui, S., Issaoui, N., Roisnel, T., Marouani, H., 2020. A tetrachlorocobaltate (II) salt with 2-amino-5-picolinium: Synthesis, theoretical and experimental characterization. J. Mol. Struct. 1207, 127781.
Taniyama, H., Yasui, B., Takehara, N., Uchida, H., 1959. Studies on chemotherapeutics for mi- cobacterium tuberculosis. XIX Synthesis and antibacterial activity of some 3-substi- tuted rhodanines. Yakugaku Zasshi 1465–1468.
W. Voegtli, US. pat. 2,857,383 (1958); Chern. Abstr. 53 (1959)624931.
Wang, J.L., Limburg, D., Graneto, M.J., Springer, J., Hamper, J.R., Liao, S., et al., 2010. The novel benzopyran class of selective cyclooxygenase-2 inhibitors. Part 2: The second clinical candidate having a shorter and favorable human half-life. J. Bioorg. Med. Chem. Lett 20, 7159–7163.
Wardakhani, W.W., Abdel-Salem, O.M.E., Elmegeed, G.A., 2008. Acta Pharm. 58, 1–14.
Wolff, S.K., Grimwood, D.J., McKinnon, J.J., Turner, M.J., Jayatilaka, D., Spackman, M.A., 2012. Crystal Explorer (Version 3.1). University of Western Australia.
Wolinski, K., Hinton, J.F., Pulay, P., 1990. Efficient implementation of the gaugeindependent atomic orbital method for NMR chemical shift calculations. J. Am. Chem. Soc. 112, 8251e8260.
Yang, J.M., Chen, C.C., 2004. GEMDOCK: a generic evolutionary method for molecular docking. Proteins Struct. Funct. Bioinforma. 55, 288–304.
Zhuo, L.G., Liao, W., Yu, Z.X., 2012. A Frontier Molecular Orbital Theory Approach to Understanding the Mayr Equation and to Quantifying Nucleophilicity and Electrophilicity by Using HOMO and LUMO Energies. Asian J. Org. Chem. 1, 336–345.